Neuron, Vol. 18, 327–338, February, 1997, Copyright ©1997 by Cell Press

ALS-Linked SOD1 Mutant G85R Mediates Damage to Astrocytes and Promotes Rapidly Progressive Disease with SOD1-Containing Inclusions

L. I. Bruijn,[1] M. W. Becher,[3,6] M. K. Lee,[3,6] K. L. Anderson,[1] N. A. Jenkins,[7] N. G. Copeland,[7] S. S. Sisodia,[3,5,6] J. D. Rothstein,[4] D. R. Borchelt,[3,6] D. L. Price,[3,5,6] and D. W. Cleveland,[1,2]

[1]Ludwig Institute for Cancer Research
[2]Departments of Medicine and Neuroscience
University of California at San Diego
La Jolla, California 92093
[3]Department of Pathology
[4]Department of Neurology
[5]Department of Neuroscience
[6]Laboratory of Neuropathology
Johns Hopkins University School of Medicine
Baltimore, Maryland 21205
[7]Mammalian Genetics Laboratory
Advanced Bioscience Laboratories Research Program
National Cancer Institute
Frederick, Maryland 21701

Summary

High levels of familial Amyotrophic Lateral Sclerosis (ALS)-linked SOD1 mutants G93A and G37R were previously shown to mediate disease in mice through an acquired toxic property. We report here that even low levels of another mutant, G85R, cause motor neuron disease characterized by an extremely rapid clinical progression, without changes in SOD1 activity. Initial indicators of disease are astrocytic inclusions that stain intensely with SOD1 antibodies and ubiquitin and SOD1-containing aggregates in motor neurons, features common with some cases of SOD1 mutant-mediated ALS. Astrocytic inclusions escalate markedly as disease progresses, concomitant with a decrease in the glial glutamate transporter (GLT-1). Thus, the G85R SOD1 mutant mediates direct damage to astrocytes, which may promote the nearly synchronous degeneration of motor neurons.

Introduction

Amyotrophic Lateral Sclerosis (ALS) is a progressive neurodegenerative disorder resulting from degeneration and death of lower motor neurons in the brain stem and spinal cord, leading to generalized weakness and muscle atrophy (Delisle and Carpenter, 1984; Banker, 1986). Of ALS cases, 5%–10% are familial, inherited in an autosomal dominant manner. The mechanisms leading to degeneration of motor neurons in familial and sporadic ALS are not clearly understood. The discovery (Rosen et al., 1993) of dominant, missense mutations (>45 such mutations are now known) in the metalloenzyme Cu–Zn superoxide dismutase (SOD1) as the primary cause of 15%–20% of familial ALS cases has focused attention on how mutants in this ubiquitously expressed enzyme cause selective death of motor neurons. Because SOD1 activity is believed to play a crucial role in regulation of oxidative stress and protection against oxygen radical-induced cellular damage (Halliwell, 1994; Yu, 1994), an initially attractive hypothesis was that SOD1-linked familial ALS resulted from free radical damage caused by diminished superoxide scavenging activity (Bowling et al., 1993; Deng et al., 1993). Consistent with this idea were reductions (50%–60%) of dismutase activity in red blood cells, lymphocytes, and brain from individuals with familial ALS mutations (Bowling et al., 1993; Deng et al., 1993; Robberecht et al., 1994) and the observation that reductions in SOD1 activity were associated with death of neurons in several culture systems (Rothstein et al., 1994a; Greenlund et al., 1995).

Despite this early focus on loss of activity as the mechanism underlying human disease, subsequent in vitro studies demonstrated that familial ALS mutations vary in their effects on enzymatic activity and, at least in some instances (such as the substitution of arginine for glycine at position 37 [G37R]), the mutant enzyme retains full specific activity (Borchelt et al., 1994). In lymphocytes from individuals with familial ALS, there is only a modest reduction in the abundance of the G37R SOD1 polypeptide, and the mutant polypeptide is fully active (Borchelt et al., 1994). Moreover, SOD1 null mice live to adulthood and to date have not been documented to develop motor neuron disease (Reaume et al., 1996).

Finally and most convincingly, lines of transgenic mice expressing either G93A or G37R human SOD1 have elevated SOD1 activity levels (4- to 14-fold that of nontransgenic littermates) and develop progressive hindlimb weakness and muscle wasting between 4 and 6 months of age. In these animals, motor neurons degenerate, often exhibiting vacuoles that have been interpreted to originate from the Golgi and endoplasmic reticulum in cell bodies of G93A mice (Dal Canto and Gurney, 1994) and from degenerating mitochondria in dendrites or axons of G37R mice (Wong et al., 1995). Disease in G93A and G37R mice requires high levels of mutant SOD1. In addition, one line of mice expressing a mutation in mouse SOD1 that is homologous in position to the familial ALS-linked G85R mutation has been reported to cause motor neuron loss and rapidly progressing disease without elevating SOD1 activity (Ripps et al., 1995).

In this report, we document that human SOD1 mutant G85R can cause dominantly inherited, rapidly progressive disease in spite of accumulation to very low levels in mice (0.2–1.0 $\times$ endogenous mouse SOD1) and without any increase or decrease in overall SOD1 activity. Despite latencies of >8 months, once initiated, motor neuron loss proceeds nearly synchronously with ~40% of large spinal motor neuron axons degenerating over a 2 week disease duration. Moreover, prominent SOD1-containing inclusions in astrocytes appear prior to clinical signs and increase markedly in abundance during disease progression, implicating astrocytes as primary targets for mutant-SOD1 mediated damage. Moreover,

the glial glutamate transporter (GLT-1), the major glutamate transporter in spinal cord, decreases during disease progression, implicating glutamate mediated excitotoxicity as a mechanism to account for the nearly synchronous degeneration of motor neurons.

Results

Low Levels of G85R Protein Accumulate in Spinal Cords of Transgenic Mice with Motor Neuron Disease

Transgenic mice were generated that carry a 12 kb genomic DNA fragment encoding a human FALS-linked SOD1 point mutation (Rosen et al, 1993) converting codon 85 from glycine to arginine (G85R; Figure 1A). From 242 potential transgenic pups, 48 founders were identified with the G85R mutant transgene. Lines were established for eight founders with low, medium, and high copy numbers (between 2 and 15 copies) as determined by tail DNA blots.

To determine the level of the human G85R mutant SOD1 that accumulated in each of the transgenic lines, spinal cord extracts were immunoblotted along with a series of known amounts of purified human erythrocyte SOD1 (Figures 1B and 1C, lanes 1–4). The amount of G85R mutant was determined using an anti-peptide polyclonal antibody specific for human SOD1 (Figure 1C), which does not bind to mouse SOD1 in extracts from normal mice (Figure 1C, lane 5). Total SOD1 (Figure 1B, lanes 5–13) was measured using a polyclonal antibody generated against a peptide identical in mouse and human SOD1. Phosphorimaging of these and a set of parallel blots (analyzing samples from four animals each for lines 148, 164, and 87 and two animals for each of the other lines) revealed that mutant SOD1 in transgenic lines (lanes 6–13) accumulated to 0.02% of total protein (~20% of endogenous mouse SOD1) for the lowest expressing line (line 46; Figure 1C, lane 11) and 0.1% of total protein (equivalent to mouse SOD1) in the highest expressing line (line 148, Figure 1C, lane 9). Using an antibody specific for mouse SOD1, levels of endogenous mouse SOD1 were unchanged in all lines (compare normal mouse in Figure 1D, lane 5 with transgenic mice in Figure 1D, lanes 6–13).

RNA blotting for levels of transgene-encoded RNA (not shown) revealed a level of RNA in the highest G85R expressing line (line 148; Figure 1C, lane 9), indistinguishable from that in a mouse line previously reported to accumulate FALS-linked mutant G37R to 5 × the level of mouse SOD1 (Wong et al., 1995). The lower level of accumulated G85R (relative to that of G37R in mice with comparable levels of mutant encoding SOD1 mRNAs) confirms in a more in vivo context the finding from transfection experiments with cultured cells (Borchelt et al., 1995) that the G85R polypeptide has a shorter half life than G37R.

Immunoblotting of extracts of various tissues, including spinal cord, cortex, brain stem, cerebellum, muscle, liver, and kidney (Figure 2A), revealed that G85R accumulated in all these tissues, as seen earlier for mutant G37R (Wong et al., 1995). Using an antibody recognizing human and mouse SOD1 (Figure 2A), mutant SOD1 accumulates in both kidney and liver to levels comparable with endogenous SOD1, whereas accumulated levels of mutant protein in cortex, brain stem, and cerebellum are lower than endogenous mouse SOD1. A similar assay of red blood cell lysates (Figure 2B, lanes 1–6) revealed that G85R SOD1 was undetectable in red blood cells (Figure 2B, lanes 2–4), whereas high levels of human SOD1 were present in transgenic mice expressing wild-type or G37R mutant SOD1 (e.g., 4 × the endogenous SOD1 level in mice expressing wild-type human SOD1; Figure 2B, lane 1). Analysis of the levels of the endogenous and G85R mutant SOD1 in spinal cords from line 148 revealed that levels of mutant SOD1 were unchanged at 1 and 3 months of age but were elevated by 2-fold at end-stage disease, whereas levels of endogenous mouse SOD1 were unaltered in these G85R transgenics (Figure 2C, middle lane) and in nontransgenic littermates (Figure 2C, bottom lane). While we cannot exclude a potential contribution of increased RNA transcription or RNA stability to the increased levels of G85R at end stage, these data strongly suggest that degradation of mutant G85R SOD1 is slowed as the animals age.

Table 1. Disease Progression in G85R SOD1 Mice (Line 148)

Astroglial							
Astrocytosis	−	−	−	−	+	+	+++
SOD1–immunoreactive inclusions	−	−	−	+	−	++	+++
Ubiquitin–immunoreactive inclusions	−	−	−	+	−	++	+++
Neuronal							
Neuronal loss	−	−	−	−	−	−	++
Axonal degeneration	−	−	−	−	+	++	+++
SOD1 and ubiquitin–immunoreactive inclusions	−	−	−	−	−	+	++
SOD1-immunoreactive perikaryal aggregates	−	−	−	+	+	+	+
Ubiquitin–immunoreactive perikaryal aggregates	−	−	−	+	+	+	+
Clinical phenotype	−	−	−	−	−	disease onset	end stage
Age in months	2	3.5	5.5	6	6.5	7.5	8

Spinal cords of animals at various ages were carefully examined for severity of ventral root degeneration, neuronal or glial inclusions; SOD and ubiquitin immunoreactivity and astrocytosis were assessed and graded as follows: +, mild degree or infrequent occurrence; ++, moderate density or moderate occurrence; and +++, marked degree and frequent.

G85R SOD1 Does Not Influence Overall SOD1 Activity

To test whether the G85R mutant affects levels of activity of the endogenous SOD1 subunits, spinal cord extracts were electrophoresed in native gels, and activity was measured by the ability of SOD1 to inhibit the conversion of nitro blue tetrazolium to formazan. In three mice from line 148, SOD1 activity was similar to that in a control animal (compare Figure 2D, lanes 5–7 with lane 4). Since the G85R subunit has previously been shown to be completely inactive in this gel assay (Borchelt et al., 1994), the constant level of activity indicates that activity of the endogenous mouse SOD1 was not altered, consistent with the constant level of mouse SOD1 polypeptide

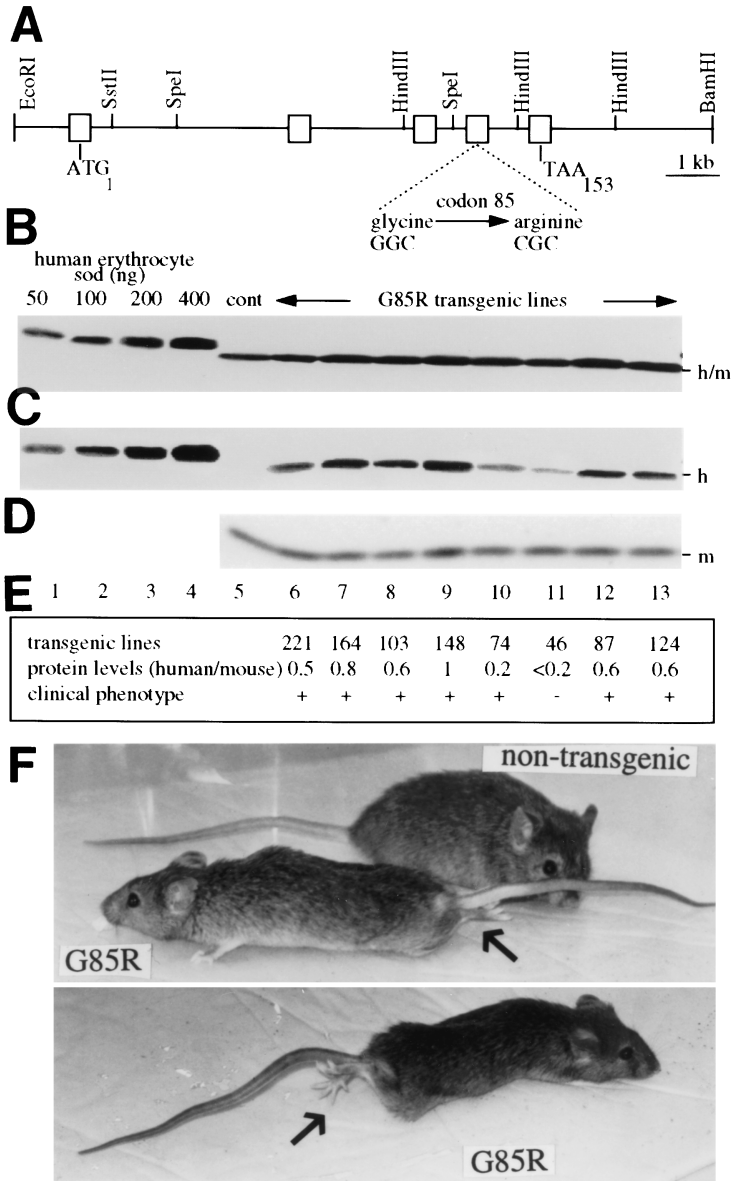

Figure 1. Low Levels of Mutant G85R SOD1 Cause Motor Neuron Disease in Multiple Lines of Transgenic Mice

(A) Schematic representation of the human SOD1 gene showing the conversion of glycine (GGC) to arginine (CGC) at codon 85 in exon 4.

(B–D) Total protein (70 μg) extracted from spinal cords of eight transgenic lines (lanes 6–13) and a nontransgenic littermate (lane 5) were electrophoresed on 15% SDS–PAGE gels and immunoblotted using rabbit polyclonal antibodies that recognize (B) a common epitope shared between human and mouse SOD1, (C) an epitope on human but not mouse SOD1, or (D) an epitope specific for mouse SOD1. All antibodies were detected with ^{125}I-labeled protein A. A series of 2-fold dilutions of purified human SOD1 was immunoblotted in parallel (lanes 1–4) to provide quantitation standards.

(E) Levels of G85R mutant SOD1 versus endogenous wild-type mouse SOD1 determined by phosphorimaging of the blots in (B) and (C).

(F) Aberrant hindlimb posture developed within 3 days of clinical onset in transgenic mice from G85R line 148. Arrows point to obviously abnormal hindlimbs.

(Figure 1D) and the observation that mutant SOD1 does not exert a dominant negative effect in vitro (Borchelt et al., 1995). The G85R polypeptide retains some activity in vivo (as reported for the mutant protein assayed in solution after expression with a baculovirus vector [Fujii et al., 1995] or in yeast (Corson et al., unpublished data]), but even if fully active in vivo, its low abundance cannot raise overall SOD1 activity significantly over that in nontransgenic control mice. Although protein levels of mutant SOD1 increase at end-stage disease (Figure 2C), endogenous mouse SOD1 activity in transgenic mice is not altered with age (compare Figure 2D, lanes 5–7 and 9–11 for transgenic animals with similar samples from control mice in lanes 4 and 8).

G85R SOD1 Causes a Late-Onset, Rapidly Progressive Motor Neuron Disease

Each of the eight lines of G85R mice was examined at different ages for clinical signs. In seven lines, mice developed hindlimb paralysis and muscle atrophy (Table 1; Figure 1F). The age of onset varied between 8–10 months for the highest expressing line (line 148–G85R levels 100% of endogenous SOD1) and 12–14 months for the lowest expressing line (line 74–G85R levels 20% of endogenous SOD1), but after onset, all mutant lines showed a uniformly rapid progression of disease. The initial sign was weakened grip strength in one hindlimb, which spread very rapidly to the other hindlimb and then to the forelimbs. Mice were completely paralyzed within 2 weeks after initial signs. In a few mice, disease advanced so rapidly that hind- and forelimbs appeared affected simultaneously. In some animals, the hindlimbs were so severely affected that the mice were unable to feed (Figure 1F) and were sacrificed before any signs of forelimb involvement. One line (line 46) expressing the lowest level of mutant SOD1 (Figure 1C, lane 11) did not develop clinical signs by 15 months.

Ten animals in line 148 were closely observed from

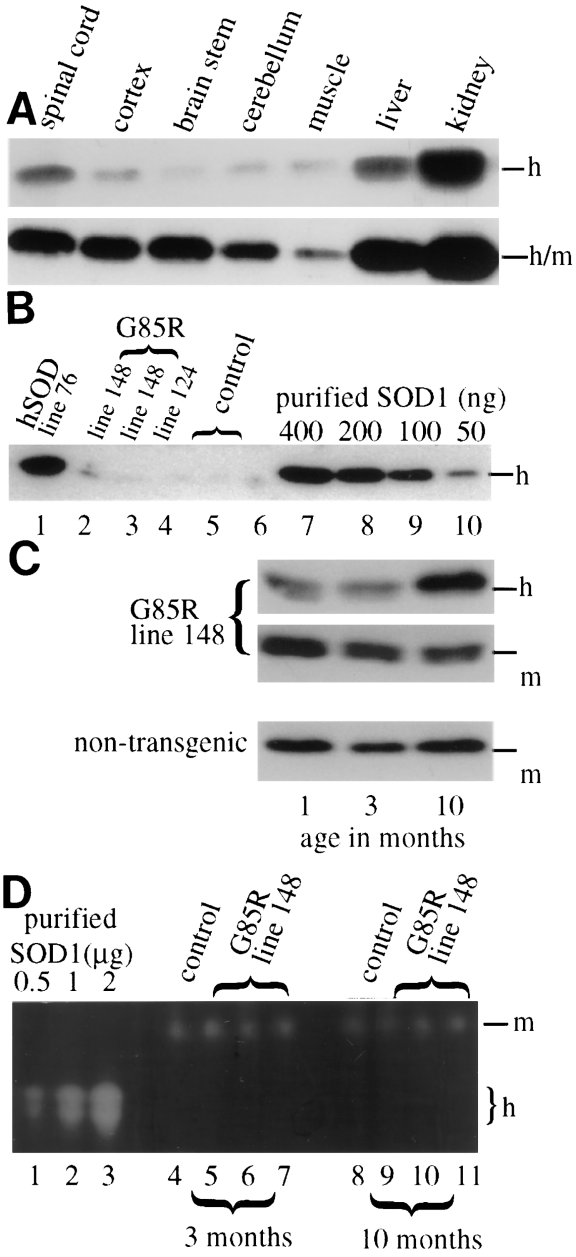

Figure 2. G85R SOD1 Accumulates in a Variety of Tissues, with a 2-Fold Increase in Spinal Cord at End-Stage Disease

(A) Total protein (70 μg) from various tissues from a 3-month-old G85R SOD1 transgenic mouse (line 148) was immunoblotted with a rabbit polyclonal antibody recognizing an epitope (top lane) specific for human SOD1 or (bottom lane) recognizing mouse and human SOD1.

(B) Immunoblots with an antibody specific for human SOD1 of extracts from red blood cells from a mouse transgenic for (lane 1) wild-type human SOD1, (lanes 2–4) G85R lines 148 (3 months old), 148 (10 months old), and 124 (10 months old), respectively, and (lanes 5 and 6) nontransgenic control mice. A series of 2-fold dilutions of purified human SOD1 were immunoblotted in parallel (lanes 7–10) to provide standards for quantitation.

(C) Total protein extracts from spinal cords of 1-, 3-, and 10-month-old (top and middle lanes) G85R, line 148 mice and (bottom lane) nontransgenic, control mice immunoblotted with antibodies recognizing an epitope specific for (top lane) human SOD1 or (middle and bottom lanes) mouse SOD1.

the time of the earliest obvious clinical signs. In all cases, within 2–3 days after appearance of hindlimb weakness, the affected hindlimb became severely paralyzed, and the limb assumed a distorted posture (Figure 1F). Within 3–4 days, the other hindlimb displayed obvious weakness, and 1–2 weeks after onset, these animals were so severely immobilized that they were unable to feed.

Evolution of Pathology: The Earliest Lesions Are SOD1-Containing Inclusions in Astrocytes and More Diffuse SOD1/Ubiquitin-Containing Aggregates in Motor Neurons

To delineate the evolution of pathology, we examined spinal cords from G85R SOD1 mice (line 148) that develop clinical signs between 8–10 months of age. No abnormalities were identified in mice <6 months of age. However, at 6 months (Table 1), early abnormalities of two types were identified.

First, round inclusions with a dense core and a clear peripheral halo were revealed by hemotoxylin and eosin (H and E) staining (Figure 3B). These inclusions resemble the Lewy bodies that are present in the cytoplasm of pigmented neurons in the substantia nigra and locus ceruleus in Parkinson's disease (Galloway et al., 1996), but in the G85R mice, these initial "Lewy body-like" inclusions were in astrocytes, not neurons, as indicated by immunoreactivy with antibodies to the astrocyte-specific glial fibrillary acidic protein (GFAP) (Figure 3A). Inclusions in astrocytes became more abundant as disease progressed. By end stage (Figure 3C), when SOD1 increased 2-fold in spinal cord extracts (Figure 2C), there was a marked increase in astrocytosis (Figure 3C, open arrow) and a ~10-fold increase in inclusions. Almost all of these were confirmed by staining with antibodies to GFAP (Figure 3C) and absence of staining with neurofilament antibodies (Figures 3D and 3E, arrows) to be within astrocytes. Similar astroglial inclusions were prominent not only in line 148 but also in three other G85R lines examined in detail (lines 103, 164, and 87). A striking finding was that throughout disease, both core and periphery of inclusions (Figure 3F) were highly immunoreactive with an antibody recognizing a common epitope in human and mouse SOD1 (Figure 3G, inset). Only the periphery of these inclusions (both in young animals or at end stage) was immunoreactive for GFAP (Figures 3A and 3C) or ubiquitin (Figure 3F, inset) antibodies. SOD1-immunoreactive inclusions were also observed in smaller cells in the white matter, which showed oligodendrocytic features and lacked GFAP (not shown). Electron microscopy of inclusions in cell bodies (Figure 4A) revealed that the core consisted of a heterogeneous mass of short (200–300 nm long), disorganized filamentous material covered with small granules (~20 nm in diameter; Figures 4B and 4C) in which organelles were entrapped, with a less dense and in some cases linear

(D) SOD1 activity in spinal cord extracts from 3- (lanes 4–7) and 10- (lanes 8–11) month-old transgenic (lanes 5–7 and 9–11) and control (lanes 4 and 8) mice determined on native gels (as described by Beauchamp and Fridovich, 1971). Lanes 1–3: a 2-fold dilution series (0.5, 1, and 2 μg) of human erythrocyte SOD1 used as quantitation standards.

array of filaments (~10 nm in diameter) at the periphery of the inclusion. The absence of reactivity to GFAP antibodies except at the periphery (Figures 3A and 3C) and the circumferential GFAP filaments observable at the edges of these aggregates strongly suggest that GFAP is not a major constituent of the filamentous material in the central domain of these aggregates.

A second type of abnormality appearing prior to clinical onset was the presence in a small number of motor neurons of a few diffuse aggregates that were intensely immunoreactive both for SOD1 (Figure 5B) and ubiquitin (Figure 5A), despite normal appearance by H and E staining. In contrast, the large majority of neurons as well as nontransgenic neurons and all neurons of G85R animals at younger ages were unreactive with ubiquitin antibodies, and these normal neurons displayed much less intense, diffuse, granular SOD1 immunoreactivity (Figure 5B, arrowheads), as previously reported (Pardo et al., 1995). Abnormalities in motor neurons progressed from diffusely localized SOD1- and ubiquitin-containing aggregates seen prior to clinical onset (Figures 5A and 5B) to rounded (Lewy body-like) or irregular inclusions visible by H and E staining in cell bodies (Figure 5C, inset). At end stage, even larger inclusions could be found in a few neurons both in the cell bodies (Figure 5E) and in proximal axonal processes (Figures 5C and 5G). Like those in astrocytes, inclusions in neuronal cell bodies and swellings of proximal processes displayed intense SOD1-immunoreactivity (Figure 5D), both in the central core and periphery. In addition, the periphery, but not the central domain, of each inclusion stained with antibodies to ubiquitin (Figure 5F). Immunocytochemistry with antibodies to multiple neurofilament epitopes (SMI-31, SMI-32, NF-H [not shown] and NF-L [Figure 5H]) revealed that neurofilaments were excluded from all of these inclusions and swellings but were often found circumferentially around an inclusion. Vacuoles like those in cell bodies, dendrites, and axons of previously reported transgenic mice expressing SOD1 mutants G93A (Gurney et al., 1994) or G37R (Wong et al., 1995) were not seen at any point in disease, and mitochondria appeared morphologically normal. Comparison of spinal cord sections of nontransgenic control and end-stage G85R animals revealed obvious loss of motor neurons in the ventral horn as the result of mutant SOD1 expression (not shown).

Neuronal abnormalities were not limited to the ventral motor neuron populations but included small neurons near the central canal and rare interneurons of the dorsal horns. Studies, to be reported in detail elsewhere, of the remainder of the central nervous system revealed similar-appearing eosinophilic inclusions in brain stem neurons and astrocytes, most prominently in the pons. No abnormalities have been identified in the cortical or subcortical structures of the brain.

Rapid, Nearly Synchronous Degeneration and Death of Large Motor Neurons Following Onset

To examine the progression of ventral motor neuron axonal degeneration, we counted the number of apparently healthy axons and the number of axons actively undergoing degeneration in ventral roots from animals before (Figure 6C), at (Figure 6D), and after (Figure 6E) appearance of clinical signs. Consistent with the earliest abnormalities in the spinal cord, no significant loss of axons was detectable prior to clinical onset (Figures 6A and 6C), although a small number (<1%) of large (>5 μm in diameter) axons in motor roots showed degeneration at 6.5 months (coincident with the earliest spinal cord pathology). However, at the time of the first clinical signs, 25% of the large motor axons were missing (Figure 6A), and of the surviving axons, 10% were actively undergoing degeneration (Figure 6B; see also Figure 6D, arrows). By the end of the 2 week clinical course, about two thirds of the large axons were absent, while 50% of those remaining were degenerating (Figure 6B). Smaller caliber axons (<5 μm in diameter) were not affected at any stage of the disease (Figure 6A). Analysis of sensory axons in the dorsal root revealed that prior to clinical onset, sensory axons were unaffected, whereas at onset, 2.5% of large axons (>5 μm in diameter) were actively degenerating or lost, with a few large swollen axons (~25 μm in diameter). The number of dorsal root axons either dying or lost increased to 7.5% of large axons at end stage.

Selective Loss of the Major Spinal Glutamate Transporter (GLT-1) during Disease Progression in G85R Mice

Excitotoxicity from excessive extracellular glutamate has been proposed as a factor in sporadic ALS, an hypothesis arising from demonstration of increased cerebrospinal fluid concentrations of glutamate early in the clinical course of ALS (Rothstein et al., 1990) and decreased glutamate transport in patients with sporadic ALS (Rothstein et al., 1992). Inactivation of glutamate is accomplished by its removal from extracellular space by glutamate transporters, three of which have been identified: GLT-1 (Pines et al., 1992) and GLAST (Storck et al., 1992) found in glia (Rothstein et al., 1994b) and EAAC1 (Kanai et al., 1993) found only in neurons (Rothstein et al., 1994b). To examine if diminished ability to sequester glutamate could be contributing to the rapid progression of G85R-mediated disease, we immunoblotted spinal cord homogenates from nontransgenic and G85R mice and measured each transporter with specific antibodies (Rothstein et al., 1994b). In four out of four animals examined, there was a 50% decrease in levels of the GLT-1 protein in spinal cord extracts from end-stage G85R mice (analyses of two of these animals are presented in Figure 7B, lane 4) compared to G85R mice at 3 months (Figure 7B, lane 3). Levels of GLT-1 were constant in age-matched control mice (Figure 7, lanes 1 and 2). Levels of EAAC1 and GLAST were below detection limits in spinal cords of normal and G85R mice, although GLAST was detected in cerebellar homogenates and EAAC1 in hippocampal homogenates. Correlation of transporter activities and immunoblotting of brain has previously shown that all three antibodies have comparable sensitivities in detecting the corresponding transporters (Rothstein et al., 1994b; 1996). These findings indicate that GLT-1 is the major glutamate transporter in spinal cord and that there is

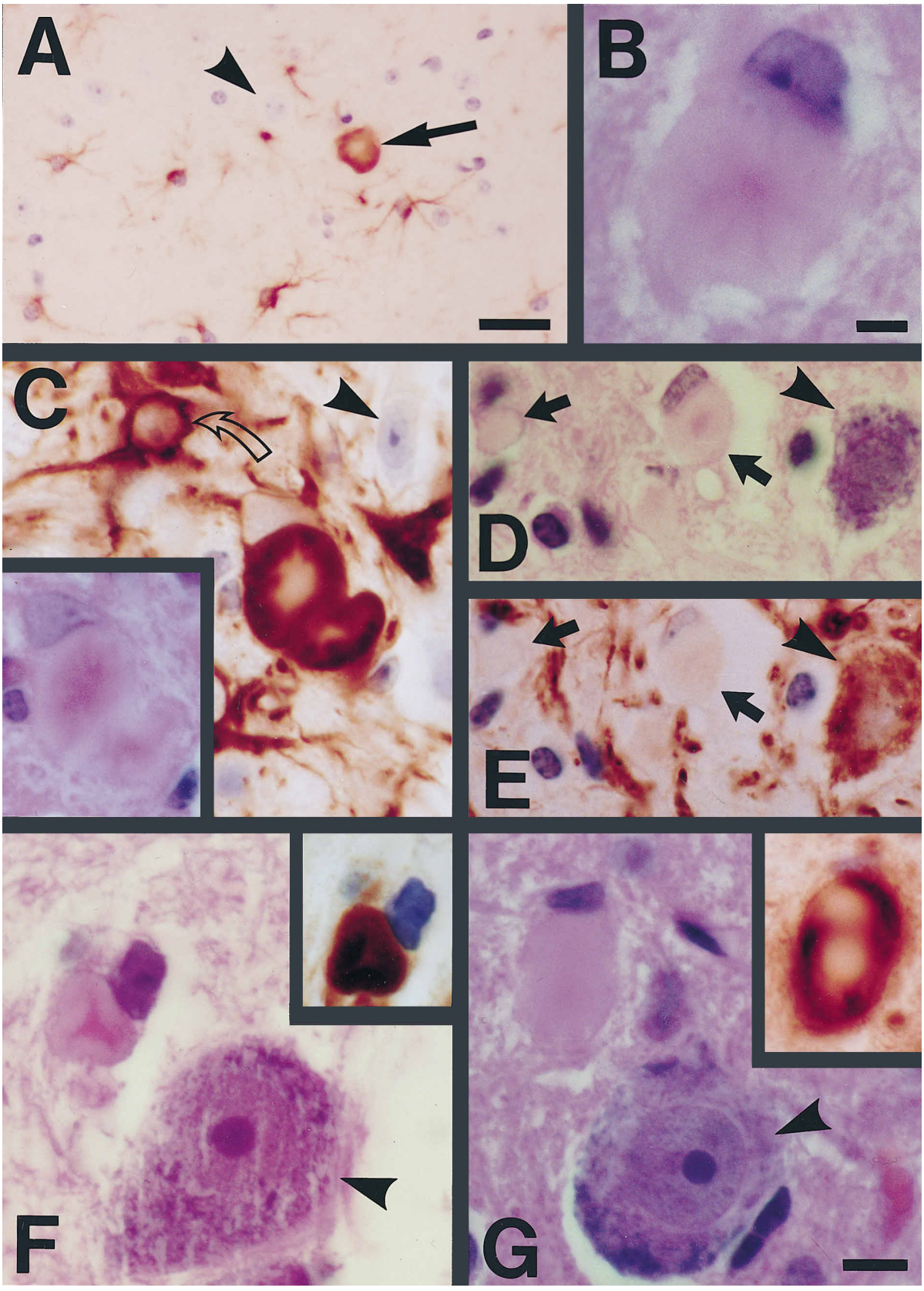

Figure 3. Lewy Body-Like Astrocytic Inclusions Strongly Immunoreactive for SOD1 Are Early Markers of Disease

reduction in its abundance as disease progresses in the G85R mice.

Discussion

We have shown that low levels of accumulated human G85R SOD1 (between 0.2 and 1.0 × the level of endogenous SOD1) are sufficient to cause severe motor neuron disease without altering the protein and activity levels of endogenous SOD1. This level of human FALS-linked mutant SOD1 is ~20-fold < the amount required to mediate disease by two previously described human FALS-linked mutants, G93A (Gurney et al., 1994) and G37R (Wong et al., 1995), indicating that G85R is significantly more toxic, at least in mice. Moreover, the most striking finding in transgenic mice expressing human G85R SOD1 is the presence of numerous inclusions in astrocytes that appear prior to similar inclusions in neurons. By end stage, when there is a 2-fold elevation in SOD1 protein in whole spinal cord extracts and a 60% loss of large axons, inclusions are approximately 10 × more abundant in astrocytes than neurons, indicating that for this mutation, astroglia are a major target of SOD1-mediated damage. Both the dense core and the periphery of both astrocytic and neuronal inclusions show high levels of SOD1 immunoreactivity. While no autopsy material is available for familial cases with the G85R mutation (N. Siddique and T. Siddique, personal communication), neuronal SOD1-positive inclusions have been described in some familial ALS patients with mutation A4V (Shibata et al., 1996), and inclusions with similar SOD1 immunoreactivity in astrocytes have also been reported in a familial ALS patient with a 2 bp deletion in the 126th codon of SOD1 leading to a frameshift and truncation of the final 27 amino acids (Kato et al., 1996). However, the demonstration here that SOD1-containing inclusions in astrocytes are early abnormalities and increase markedly in abundance after disease onset provides strong support for the view that at least some of the familial ALS-linked SOD1 mutants mediate disease by direct affects on astrocytes, in both human and murine disease.

Although it is not obvious how inclusions originate, the finding that these inclusions contain abundant SOD1 polypeptides, both in the core and periphery, implicates aberrant accumulation of mutant protein, perhaps as a result of an altered conformation that resists the ubiquitin-mediated degradation pathway. Whether toxicity arises from the physical presence of the inclusion or from aberrant chemistry mediated by the SOD1 in these aggregates remains unresolved. An additional key question not yet resolved is whether the SOD1 in these inclusions represents the mutant subunit, endogenous SOD1, or a mixture of both. We have attempted to answer this using peptide antibodies specific for human or mouse SOD1; however, they have failed to detect the corresponding proteins by immunocytochemistry, despite repeated attempts and their high sensitivity on immunoblots. Since expression of wild-type SOD1 alone does not form such aggregates even at 12 × the normal level, it must be that the mutant protein induces aggregate formation. However, neither the level of endogenous mouse protein nor its activity in whole tissue extracts is altered even at end stage, indicating that overall degradation and activity of endogenous mouse SOD1 is not significantly affected by the presence of the mutant subunit. Of course, as both activity and protein levels of mouse and mutant SOD1 are measures of whole spinal cord, we cannot exclude the possibility that there are regional differences in SOD1 activity and accumulation. Indeed, the SOD1-containing inclusions, primarily in astrocytes but also in motor neurons, offer direct experimental support for the possibility that toxicity of some SOD1 mutants may arise from mutant-mediated aggregation and the corresponding mislocalization of SOD1 (including local loss of activity). This cannot be the only affect of the mutants, however, since complete loss of SOD1 does not result in motor neuron disease (Reaume et al., 1996).

Central to understanding the mechanism of neuronal death in SOD1-linked familial ALS is the identity of the toxic property or properties that lead to familial ALS. One hypothesis put forward by Beckman and colleagues (Beckman et al., 1993) is that the mutant subunits unfold slightly, allowing increased access of peroxynitrite (formed spontaneously from nitric oxide [NO] and superoxide anion [O_2^-]) to the enzyme-bound copper, which in turn uses peroxynitrite to nitrate tyrosine residues on proteins. A second hypothesis holds that the mutants catalyze the formation of hydroxyl radicals from hydrogen peroxide via a process called the Fenton reaction. Hydroxyl radicals have been proposed to damage a variety of cellular targets including SOD1, mitochondrial membranes (via lipid peroxidation), and glutamate transporters (via oxidation) (Pogun et al., 1994). In vitro, at least two mutations can increase the rate of hydroxyl

(A and B) Lewy body-like cytoplasmic inclusions in astrocytes, consisting of a pale periphery and dense central core seen by (B) H and E as one of the earliest pathological findings in a 6-month-old transgenic mouse (line 148) expressing G85R SOD1.

(A) The astrocytic nature of the cells that contain these inclusions is demonstrated by the peripheral, halo-like staining with antibodies to GFAP (arrow). Arrowhead points to a nucleus of an adjacent motor neuron.

(C) Individual inclusions (H and E, inset) from an end-stage G85R animal, and destaining–restaining with (C) antibodies to GFAP reveals that the periphery of these inclusions are immunoreactive for GFAP. Open Arrow points to a reactive astrocyte. Arrowhead points to an adjacent motor neuron nucleus.

(D and E) H and E view (D) of an end-stage G85R spinal cord revealing (arrows) two Lewy-body like inclusions. (E) Destaining and restaining of the same section as in (D) using an antibody to NF-L demonstrates that both inclusions are not in neurons. Arrowhead in (D) and (E) points to a motor neuron.

(F and G) H and E staining reveals an astrocytic inclusion and (arrowhead) a normal motor neuron in a spinal cord section from G85R (F) line 148 or (G) line 87 animals after clinical onset. Inset in F: the same astrocyte as in (F) after destaining and restaining with an antibody recognizing human and mouse SOD1. Inset in G: the same astrocyte as in (G) after destaining and restaining with an antibody to ubiquitin. Scale bars: in A, 25 μm; B, 5 μm; and C–G, 10 μm.

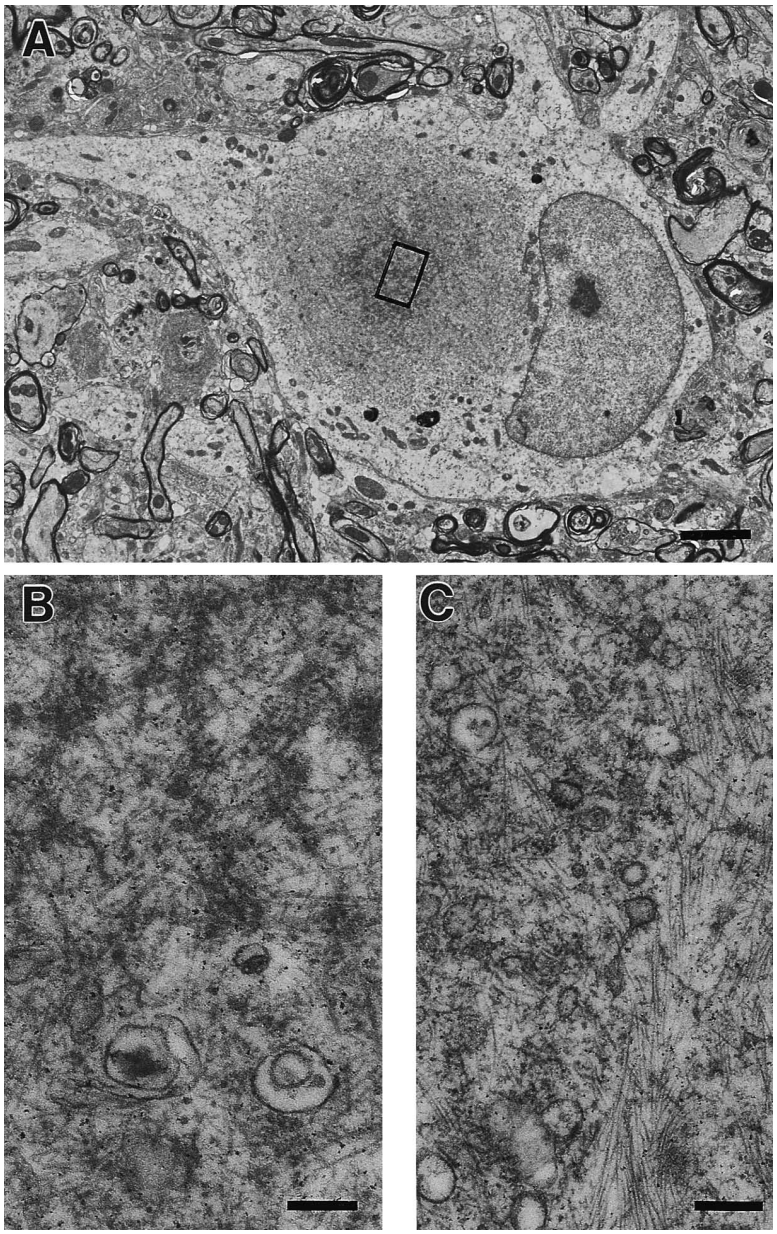

Figure 4. Electron Microscopy Reveals That the SOD1-Reactive Lewy Body-Like Inclusions Are Intracellular with a Disorganized Filamentous Core and Circumferential Intermediate Filaments

(A) An intracellular inclusion with a dense core consisting of a heterogeneous mass of short (200–300 nm long), disorganized filamentous material. Scale bar, 25 nm.

(B) Higher magnification of the area highlighted in (A). Small granules and surrounding filaments (together ~20 nm in diameter) contain entrapped organelles.

(C) The more linear array of 10 nm filaments (presumably GFAP intermediate filaments) at the periphery of the inclusion. Scale bars in (B) and (C), 200 nm.

radical formation, probably due to increased availability of the active Cu^{2+} site to H_2O_2 (Wiedau-Pazos et al., 1996). However, there is as yet no in vivo support (in human tissues or in mouse models) for either hypothesis. Moreover, that mice expressing G85R SOD1 differ clinically (later onset plus rapid and synchronous motor neuron loss after onset) and pathologically (numerous astroglial inclusions and absence of vacuoles) from G93A and G37R SOD1 mice may be explained by differences 1) in the toxic properties of the mutants, such as preferential, conformation-dependent use of peroxide, peroxynitrite, or other abnormal substrates and 2) the specific vulnerabilities of different cell types (i.e., glia or neurons) to each mutant's toxic effects.

That SOD1-mediated damage to the astrocytes is the most prominent early abnormality in the preclinical period of G85R-mediated disease offers strong support for the idea that molecular targets exist within astrocytes that can be damaged by mutant SOD1. Dysfunction of astrocytes could have significant consequences. These cells provide molecules (e.g., trophic factors and nutrients, etc.) that crucial for neuronal viability (Oppenheim et al., 1988; Lin et al., 1993). Moreover, these cells influence the microenviroment in the neuropil through scavenging of extracellular neurotransmitters, such as glutamate. The primary mechanism for the inactivation of glutamate is its removal from the extracellular space by glutamate transporters. One of these, GLT-1, is found only in glia (Rothstein et al., 1994b). A second, GLAST, was initially thought to be present in glia and neurons but more recently has been argued to be only in glia (Rothstein et al., 1996), while the third, EAAC1, is found

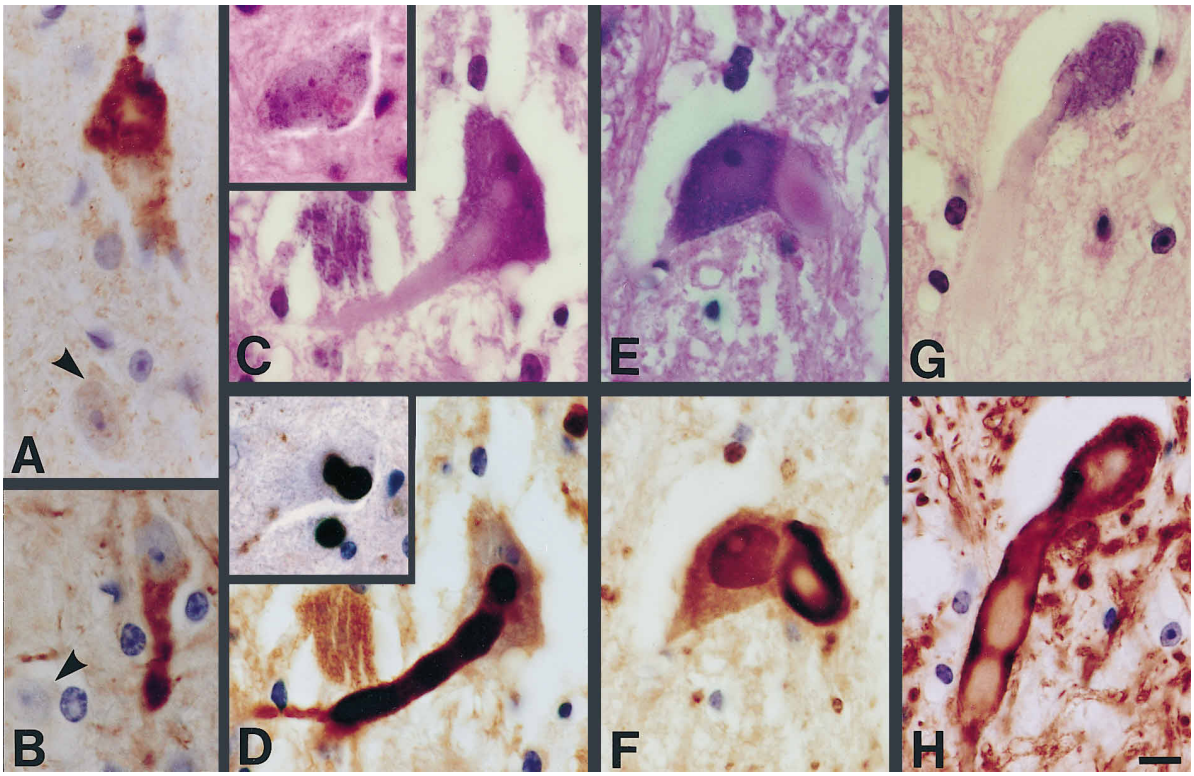

Figure 5. SOD1 and Ubiquitin Immunoreactive Inclusions in Neuronal Cell Bodies and Processes in G85R Transgenic Mice Are Early Hallmarks of Disease That Increase in Abundance at End-Stage Disease

(A and B) Early neuronal abnormalities in G85R transgenic animals consist of diffusely localized cytoplasmic aggregates that are immunoreactive with (A) ubiquitin or (B) SOD1 antibodies. In both cases, these cytoplasmic aggregates display significantly more intense immunoreactivity than that seen in normal, unaffected neurons (denoted by arrowheads).

(C–H) Neurons from G85R transgenic animals following clinical onset reveal intracellular inclusions distinguishable by ([C], [E], and [G]) H and E staining in ([C], inset, and [E]) cell bodies and in ([C] and [G]) processes. Destaining and restaining of the same neurons with antibodies to (D) SOD1, (F) ubiquitin, or (H) NF-L demonstrate that the core of the inclusions are intensely reactive with SOD1 antibodies, while only the periphery is reactive with antibodies to ubiquitin or NF-L. (C), (D), (G), and (H): G85R line 148; (E) and (F): G85R line 87. Scale bar in A–H, 10 μm.

only in neurons (Rothstein et al., 1994b). We have shown here that GLT-1 is the most abundant glutamate transporter in spinal cords and that levels of it are decreased in end-stage G85R mice, a finding that is strikingly similar to that observed in patients with sporadic ALS (Rothstein et al., 1995). Moreover, loss of either glial transporter, GLT-1 or GLAST, via chronic intraventricular antisense oligonucleotide administration has been shown to produce a progressive motor deficit in rats (Rothstein et al., 1996). Indeed, in these antisense experiments, obvious motor deficits arose when GLT-1 levels were reduced by only 50%, a reduction similar to the loss in GLT-1 arising during G85R SOD1-mediated disease. Since impairments in the transport of glutamate from the neuropil in the ventral horn could render motor neurons vulnerable to excitotoxicity, a plausible explanation for the rapid, nearly synchronous axonal degeneration and neuronal loss at end stage (at a time that the mutant protein increases in overall abundance) is that G85R-induced damage to astrocytes, necessary for the viability of neurons, mediates the rapid spread of disease after onset.

Experimental Procedures

Construction of Transgenic Mice Expressing Mutant G85R Human SOD1

The G85R mutation was engineered into the human SOD1 gene (a 12 kb EcoRI–BamHI genomic DNA fragment) by PCR/oligonucleotide primer-directed mutagenesis strategy as described by Wong et al. (1995), starting from a previously characterized plasmid, pHGSOD-SVneo (Epstein et al., 1987) encoding wild-type human SOD1. Transgenic founder mice were identified by blotting of DNA isolated from mouse tail using a human SOD1 cDNA as a probe.

Quantitation of G85R SOD1 in Lines of Transgenic Mice

Whole spinal cords from transgenic and control mice were homogenized in buffer containing 50 mM Tris, 150 mM NaCl, 5 mM EDTA, 1% SDS, 1% NP40, and 1 mM each of leupeptin, pepstatin, and chymostatin. Homogenates were sonicated for 20 s, boiled for 10 min, and clarified by centrifugation at 16,000 × g, and supernatants were transferred to new tubes. After determining the protein concentration using a bicinchonic acid (BCA) protein assay (Pierce Chemical Company, Rockford, Illinois), 70 μg of total protein were loaded on 15% polyacrylamide gels, electrophoresed, and transferred to nitrocellulose filters (Lopata and Cleveland, 1987). Immunoblots were reacted with polyclonal antipeptide antibodies (CYASGEPVVL SGQIT corresponding to residues 24–36 from mouse SOD1 or CESN

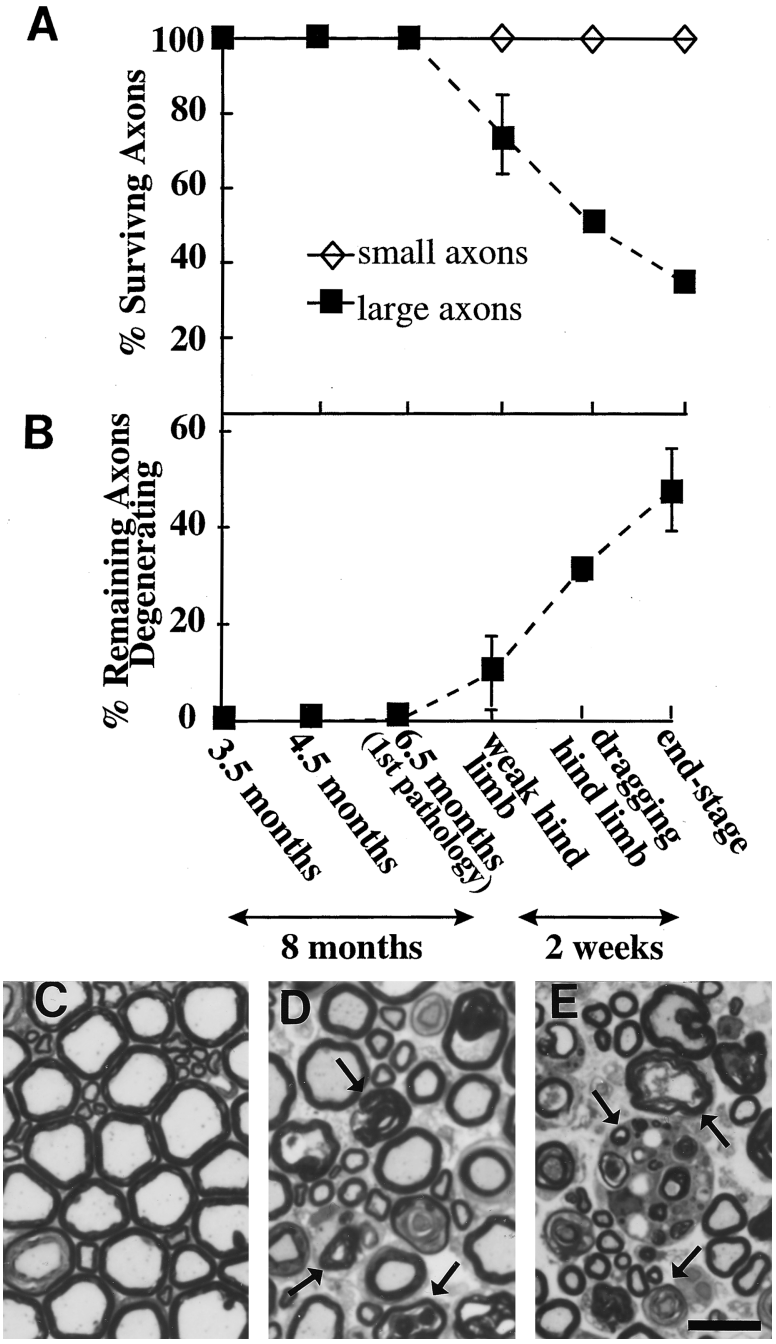

Figure 6. Rapid Degeneration and Loss of Large Motor Axons in Ventral Roots of G85R SOD1 Mice Beginning at Onset of Clinical Signs

(A and B) Percentage of (A) surviving (both healthy and degenerating) large (>5 μm) and small caliber axons in L4 ventral roots from G85R, line 148 transgenic mice measured at ages prior to clinical symptoms (3.5–6.5 M), at onset of clinical signs, and at end stage. A dramatic loss of large caliber axons is seen beginning with disease onset; small caliber axons are unaffected at all ages.

(B) Percentage of remaining large axons actively degenerating. No degeneration was observed in small axons.

(C–E) Representative images of ventral roots from (C) a 4.5-month-old animal prior to onset of pathology, (D) an 8-month-old animal at clinical onset, and (E) an end-stage (8.5-month-old) animal. Scale bar, 12 μm.

GPVKVWGSIK corresponding to residues 24–36 from human SOD1) or an antipeptide antibody (Pardo et al., 1995) generated against a sequence identical in human and mouse SOD1 (CYDDLGKGGNEE STK corresponding to residues 124–136). Bound primary antibody was detected with ^{125}I-labeled protein A. Quantitation was achieved by immunoblotting a dilution series of known amounts of purified human erythrocyte SOD1 (Sigma, St. Louis) in parallel. Signals were quantified using a Molecular Dynamics Phosphorimager (Sunnyvale, California).

Detection of Blood SOD1

Blood from nontransgenic mice, mice expressing wild-type human SOD1, and G85R transgenic mice was hemolyzed, extracted with ethanol and chloroform (L'Abbe and Fischer, 1990), and clarified by centrifugation at 10,000 × g. The supernatant (red blood cell lysate) was electrophoresed on a 15% polyacrylamide gel, transferred onto nitrocellulose, and immunoblotted with an antibody specific for human SOD1.

Measurement of SOD1 Activity

The spinal cords from control and transgenic mice were homogenized in buffer containing 20 mM Tris–HCl (pH 7.2), 1 mM EDTA, and 1% Triton X-100. After centrifugation at 10,000 × g for 5 min, the supernatant was electrophoresed on a 7.5% polyacrylamide gel, and SOD1 activities were determined as previously reported (Beauchamp and Fridovich, 1971).

Measurement of Levels of Glutamate Transporters GLT-1, GLAST, and EEAC1

Extracts of whole spinal cord from control and transgenic mice were prepared as described above and electrophoresed on 7.5%

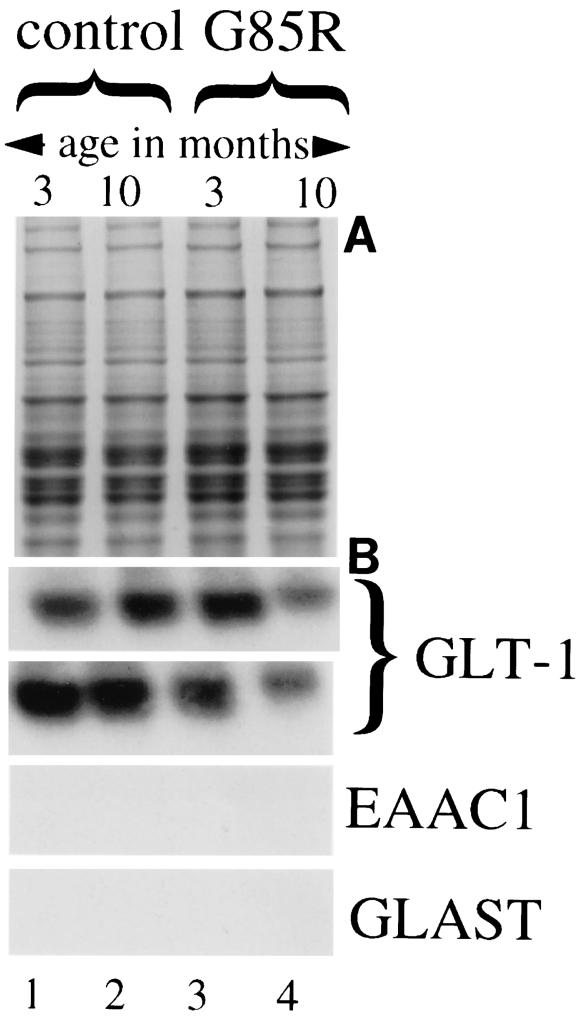

Figure 7. The Astrocytic Glutamate Transporter GLT-1 Is Lost during Disease Progression in G85R SOD1 Transgenic Mice

(A) Coomassie blue–stained gel of total spinal cord extracts from 3- or 10-month-old control or G85R (line 148) transgenic mice.

(B) Immunoblots of spinal cord extracts as in (A), probed for glutamate transporters GLT-1, EAAC1, or GLAST. The lower lanes of GLT-1 are an analysis from a second set of mice analyzed in parallel.

polyacrylamide gels, transferred to nitrocellulose filters, and reacted with rabbit polyclonal antipeptide antibodies recognizing GLT-1, GLAST, and EAAC1 (Rothstein et al., 1994b).

Histopathological and Immunocytochemical Analyses

Mice anesthetized with an intraperitoneal injection of 0.02 cc/g Avertin (tribromoethanol and tertamyl alcohol) were sacrificed by transcardiac perfusion with 4% paraformaldehyde in 0.1 M sodium phosphate (pH 7.6). Spinal cords were removed, postfixed in the same solution, embedded in paraffin, sectioned (10 μm), and stained with H and E, cresyl violet, and Bielschowski silver methods. Deparaffinized sections were processed for immunocytochemistry with the peroxidase–antiperoxidase method using antibodies recognizing: phosphorylated and nonphosphorylated neurofilaments (SMI-31 and SMI-32, respectively, Sternberger Monoclonals Inc., Baltimore); carboxyl termini of neurofilament light (NF-L) and heavy (NF-H) subunits (Xu et al., 1993), GFAP (DAKO, Carpinteria, California), ubiquitin (DAKO and Chemicon, Temecula, California) and human–mouse SOD1 (Pardo et al., 1995). Following rehydration, sections were quenched for 30 min in methanol and 0.3% hydrogen peroxide, rinsed in phosphate-buffered saline, and incubated overnight in the primary antibody. Immunoreactivity was visualized with diaminobenzidine, and sections were counterstained with hematoxylin. For characterization of inclusion bodies, H and E–stained sections of spinal cords from end-stage animals were examined and photographed by light microscopy. Coverslips were removed, slides were rinsed in xylene, 100%, 95%, and 70% alcohol, decolorized with 1% HCl in 70% ethanol for a few minutes, and stained by standard immunocytochemical methods.

Electron Microscopy

Spinal cords and roots were dissected from transcardially perfused animals and postfixed in 4% paraformaldehyde and 1% gluteraldehyde. Subsequently, tissues were incubated in 2% osmium tetroxide in 0.05 M cacodylate for 3.5 hr, washed, dehydrated, and embedded in Epon–Araldite resin (Ernest F. Fullam, Inc., Latham, New York). Thick (0.75 μm) sections stained with toludine blue were examined by light microscopy, while thin (70 nm) sections were stained with lead citrate–uranyl acetate and examined by electron microscopy.

Quantitation of Motor Neuron Degeneration

Large (>5 μm diameter) and small (<5 μm diameter) axons were counted in cross sections of L4 ventral roots from transgenic mice at 3.5, 4.5, and 6.5 months of age, as well as transgenic mice showing the first signs of hindlimb weakness and at end-stage disease. The number of surviving axons was determined as a percentage of the total number of large or small axons in an average of five control mice. The number of degenerating axons was determined as a percentage of the total number of surviving (both healthy and degenerating) axons. Two animals were used for each time point.

Acknowledgments

We thank Ms. Marilyn Peper for her assistance with immunocytochemical preparations. This work has been supported by grants from the NIH (NS 27036 to Dr. Cleveland and AG 05146 to Dr. Price) and the Amyotrophic Lateral Sclerosis Association (to Drs. Cleveland, Borchelt, and Lee). Dr. Bruijn receives support as a Postdoctoral Fellow of the Muscular Dystrophy Association. Dr. Price is the recipient of a Leadership and Excellence in Alzheimer's Disease (LEAD) Award from NINDS (NS 10580).

Received December 2, 1996; revised January 10, 1997.

References

Banker, B.Q. (1986). The pathology of the motor neuron diseases. In Myology. A. G. Engel and B. Q. Banker, eds. (New York: McGraw-Hill), pp. 2031–2066.

Beauchamp, C., and Fridovich, I. (1971). Superoxide dismutase: improved assays and an assay applicable to acrylamide gels. Ann. Biochem. *44*, 276–287.

Beckman, J.S., Carson, M., Smith, C.D., and Koppenol, W.H. (1993). ALS, SOD and peroxynitrite. Nature *364*, 584.

Borchelt, D.R., Lee, M.K., Slunt, H.S., Guarnieri, M., Xu, Z.S., Wong, P.C., Brown, R.H., Jr., Price, D.L., Sisodia, S.S., and Cleveland, D.W. (1994). Superoxide dismutase 1 with mutations linked to familial amyotrophic lateral sclerosis possesses significant activity. Proc. Natl. Acad. Sci. USA *91*, 8292–8296.

Borchelt, D.R., Guarnieri, M., Wong, P.C., Lee, M.K., Slunt, H.S., Xu, Z.S., Sisodia, S.S., Price, D.L., and Cleveland, D.W. (1995). Superoxide dismutase 1 subunits with mutations linked to familial amyotrophic lateral sclerosis do not affect wild-type subunit function. J. Biol. Chem. *270*, 3234–3238.

Bowling, A.C., Schulz, J.B., Brown, R.H., Jr., and Beal, M.F. (1993). Superoxide dismutase activity, oxidative damage, and mitochondrial energy metabolism in familial and sporadic amyotrophic lateral sclerosis. J. Neurochem. *61*, 2322–2325.

Dal Canto, M.C., and Gurney, M.E. (1994). Development of central nervous system pathology in a murine transgenic model of human amyotrophic lateral sclerosis. Am. J. Pathol. *145*, 1271–1279.

Delisle, M.B., and Carpenter, S. (1984). Neurofibrillary axonal swellings and amyotropic lateral sclerosis. J. Neurol. Sci. *63*, 241–250.

Deng, H.-X., Hentati, A., Tainer, J.A., Iqbal, Z., Cayabyab, A., Hung, W.-Y., Getzoff, E.D., Hu, P., Herzfeldt, B., Roos, R.P., Warner, C., and Siddique, T. (1993). Amyotrophic lateral sclerosis and structural defects in Cu,Zn superoxide dismutase. Science *261*, 1047–1051.

Epstein, C.J., Avraham, K.B., Lovett, M., Smith, S., Elroy-Stein, O., Rotman, G., Bry, C., and Groner, Y. (1987). Transgenic mice with increased Cu/Zn-superoxide dismutase activity: animal model of dosage effects in Down syndrome. Proc. Natl. Acad. Sci. USA *84*, 8044–8048.

Fujii, J., Myint, T., Seo, H.G., Kayanoki, Y., Ikeda, Y., and Taniguchi, N. (1995). Characterization of wild-type and amyotrophic lateral sclerosis-related mutant Cu,Zn-superoxide dismutatses overproduced in baculovirus-infected insect cells. J. Neurochem. *64*, 1456–1461.

Galloway, P., Mulvihill, P., and Perry, G. (1996). Filaments of Lewy bodies contain insoluble cytoskeletal elements. Am. J. Pathol. *140*, 809–822.

Greenlund, L.J., Deckwerth, T.L., and Johnson, E.M., Jr. (1995). Superoxide dismutase delays neuronal apoptosis: a role for reactive oxygen species in programmed neuronal death. Neuron *14*, 303–315.

Gurney, M.E., Pu, H., Chiu, A.Y., Dal Canto, M.C., Polchow, C.Y., Alexander, D.D., Caliendo, J., Hentati, A., Kwon, Y.W., and Deng, H.X. (1994). Motor neuron degeneration in mice that express a human Cu,Zn superoxide dismutase mutation. Science *264*, 1772–1775.

Halliwell, B. (1994). Free radicals, antioxidants, and human disease: curiosity, cause, or consequence? Lancet *344*, 721–724.

Kanai, Y., Smith, C.P., and Hediger, M.A. (1993). A new family of neurotransmitter transporters: the high-affinity glutamate transporters. FASEB *7*, 1450–1459.

Kato, S., Shimono, M., Watanabe, Y., Nakashima, K., Takahashi, K., and Ohama, E. (1996). Familial Amyotrophic Lateral Sclerosis with a two base pair deletion in superoxide dismutase 1 gene: multisystem degeneration with intracytoplasmic hyaline inclusions in astrocytes. J. Neuropathol Exp. Neurol. *55*, 1089–1101.

L'Abbe, M., and Fischer, P. (1990). Automated assay of superoxide dismutase in blood. Methods Enzymol. *38*, 232–237.

Lin, L.-F.H., Doherty, D.H., Lile, J.D., Bektesh, S., and Collins, F. (1993). GDNF: a glial cell line-derived neurotrophic factor for midbrain dopaminergic neurons. Science *260*, 1130–1132.

Lopata, M.A., and Cleveland, D.W. (1987). In vivo microtubules are copolymers of available beta-tubulin isotypes: localization of each of six vertebrate beta-tubulin isotypes using polyclonal antibodies elicited by synthetic peptide antigens. J. Cell Biol. *105*, 1707–1720.

Oppenheim, R.W., Haverkamp, L.J., Prevette, D., McManaman, J.L., and Appel, S.H. (1988). Reduction of naturally occurring motoneuron death in vivo by a target-derived neurotrophic factor. Science *240*, 919–922.

Pardo, C.A., Xu, Z., Borchelt, D.R., Price, D.L., Sisodia, S.S., and Cleveland, D.W. (1995). Superoxide dismutase is an abundant component in cell bodies, dendrites, and axons of motor neurons and in a subset of other neurons. Proc. Natl. Acad. Sci. USA *92*, 954–958.

Pines, G., Danbolt, N.C., Bjoras, M., Zhang, Y., Bendahan, A., Eide, L., Koepsell, H., Storm-Mathisen, J., Seeburg, E., and Kanner, B.I. (1992). Cloning and expression of a rat brain L-glutamate transporter. Nature *360*, 464–467.

Pogun, S., Dawson, V, and Kuhar, M.J. (1994). Nitric oxide inhibits L-glutamate transport in synaptosomes. Synapse *18*, 21–26.

Reaume, A.G., Elliott, J.L., Hoffman, E.K., Kowall, N.W., Ferrante, R.J., Siwek, D.F., Wilcox, H.M., Flood, D.G., Beal, M.F., Brown, R.H., Jr., Scott, R.W., and Snider, W.D. (1996). Motor neurons in Cu/Zn superoxide dismutase-deficient mice develop normally but exhibit enhanced cell death after axotomy. Nature Genet. *13*, 43–47.

Ripps, M.E., Huntley, G.W., Hof, P.R., Morrison, J.H., and Gordon, J.W. (1995). Transgenic mice expressing an altered murine superoxide dismutase gene provide an animal model of amyotrophic lateral sclerosis. Proc. Natl. Acad. Sci. USA *92*, 689–693.

Robberecht, W., Sapp, P., and Viaene, M. (1994). Cu/Zn superoxide dismutase activity in familial and sporadic amyotrophic lateral sclerosis. J. Neurochem. *62*, 384–387.

Rosen, D.R., Siddique, T., Patterson, D., Figlewicz, D.A., Sapp, P., Hentati, A., Donaldson, D., Goto, J., O'Regan, J.P., Deng, H.X., and Brown, R. (1993). Mutations in Cu/Zn superoxide dismutase gene are associated with familial amyotropic lateral sclerosis. Nature *362*, 59–62.

Rothstein, J.D., Tsai, G., Kuncl, R.W., Clawson, L., Cornblath, D.R., Drachman, D.B., Pestronk, A., Stauch, B. L., and Coyle, J.T. (1990). Abnormal excitatory amino acid metabolism in amyotrophic lateral sclerosis. Ann. Neurol. *28*, 18–25.

Rothstein, J.D., Martin, L.J., and Kuncl, R.W. (1992). Decreased glutamate transport by the brain and spinal cord in amyotrophic lateral sclerosis. N. Engl. J. Med. *326*, 1464–1468.

Rothstein, J.D., Bristol, L.A., Hosler, B., Brown, R.H., Jr., and Kuncl, R.W. (1994a). Chronic inhibition of superoxide dismutase produces apoptotic death of spinal neurons. Proc. Natl. Acad. Sci. USA *91*, 4155–4159.

Rothstein, J.D., Martin, L., Levey, A.I., Dykes-Hoberg, M., Jin, L., Wu, D., Nash, N., and Kuncl, R.W. (1994b). Localization of neuronal and glial glutamate transporters. Neuron *13*, 713–725.

Rothstein, J.D., Van Kammen, M., Levey, A.I., Martin, L.J., and Kuncl, R.W. (1995). Selective loss of glial glutamate transporter GLT-1 in amyotrophic lateral sclerosis. Ann. Neurol. *38*, 73–84.

Rothstein, J.D., Dykes-Hoberg, M., Pardo, C.A., Bristol, L.A., Jin, L., Kuncl, R.W., Kanai, Y., Hediger, M.A., Wang Y., Schielke, J., and Welty, D. (1996). Knockout of glutamate transporters reveals a major role for astroglial transport in excitotoxicity and clearance of glutamate. Neuron *16*, 674–686.

Shibata, N., Hirano, A., Kobayashi, M., Siddique, T., Deng, H.-X., Hung, W.-Y., Kato, T., and Asayama, K. (1996). Intense superoxide dismutase-1 immunoreactivity in intraplasmic hyaline inclusions of familial amyotrophic lateral sclerosis with posterior column involvement. J. Neuropathol. Exp. Neurol. *55*, 481–490.

Storck, T., Schulte, S., Hofmann, K., and Stoffel, W. (1992). Structure, expression, and functional analysis of a Na-dependent glutamate/aspartate transporter from rat brain. Proc. Natl. Acad. Sci. USA *89*, 10955–10959.

Wiedau-Pazos, M., Goto, J.J., Rabizadeh, S., Gralla, E.D., Roe, J.A., Valentine, J.S., and Bredesen, D.E. (1996). Altered reactivity of superoxide dismutase in familial amyotrophic lateral sclerosis. Science *271*, 515–518.

Wong, P.C., Pardo, C.A., Borchelt, D.R., Lee, M.K., Copeland, N.G., Jenkins, N.A., Sisodia, S.S., Cleveland, D.W., and Price, D.L. (1995). An adverse property of a familial ALS-linked SOD1 mutation causes motor neuron disease characterized by vaculolar degeneration of mitochondria. Neuron *14*, 1105–1116.

Xu, Z., Cork, L.C., Griffin, J.W., and Cleveland, D.W. (1993). Involvement of neurofilaments in motor neuron disease. J. Cell Sci. Suppl. *17*, 101–108.

Yu, B.P. (1994). Cellular defenses against damage from reactive oxygen species. Physiol. Rev. *74*, 139–162.